

See discussions, stats, and author profiles for this publication at: <https://www.researchgate.net/publication/259738407>

BioFET–SIM: A Tool for the Analysis and Prediction of Signal Changes in Nanowire–Based Field Effect Transistor Biosensors

Chapter · January 2014

DOI: 10.1007/978-3-319-02772-2_3

CITATIONS

2

READS

1,560

6 authors, including:



Martin Hediger

University of Zurich

22 PUBLICATIONS 49 CITATIONS

SEE PROFILE



Karen L. Martinez

University of Copenhagen

95 PUBLICATIONS 2,494 CITATIONS

SEE PROFILE



Mads Brandbyge

Technical University of Denmark

250 PUBLICATIONS 17,904 CITATIONS

SEE PROFILE



Luca De Vico

Università degli Studi di Siena

82 PUBLICATIONS 4,921 CITATIONS

SEE PROFILE

Chapter 3

BioFET-SIM: A Tool for the Analysis and Prediction of Signal Changes in Nanowire-Based Field Effect Transistor Biosensors

Martin R. Hediger, Karen L. Martinez, Jesper Nygård, Mads Brandbyge, Jan H. Jensen, and Luca De Vico

Abstract Biosensors based on nanowire field effect transistor (FET) have received much attention in recent years as a way to achieve ultra-sensitive and label-free sensing of molecules of biological interest. The BioFET-SIM computer model permits the analysis and interpretation of experimental sensor signals through its web-based interface www.biofetsim.org. The model also allows for predictions of the effects of changes in the experimental setup on the sensor signal. After an introduction to nanowire-based FET biosensors, this chapter reviews the theoretical basis of BioFET-SIM models describing both single and multiple charges on the analyte. Afterwards the usage of the interface and its relative command line version is briefly shown. Finally, possible applications of the BioFET-SIM model are

M.R. Hediger • J.H. Jensen • L. De Vico (✉)

Department of Chemistry, University of Copenhagen, Universitetsparken 5, DK-2100 Copenhagen, Denmark

e-mail: martin@chem.ku.dk; jhjensen@chem.ku.dk; luca@chem.ku.dk

K.L. Martinez

Bionanotechnology and Nanomedicine Laboratory, Department of Chemistry, University of Copenhagen, Universitetsparken 5, DK-2100 Copenhagen, Denmark

Nano-Science Center, University of Copenhagen, Universitetsparken 5, DK-2100 Copenhagen, Denmark

e-mail: martinez@nano.ku.dk

J. Nygård

Niels Bohr Institute, Center for Quantum Devices, University of Copenhagen, Universitetsparken 5, DK-2100 Copenhagen, Denmark

Nano-Science Center, University of Copenhagen, Universitetsparken 5, DK-2100 Copenhagen, Denmark

e-mail: nygard@nbi.ku.dk

M. Brandbyge

DTU Nanotech, Department of Micro and Nanotechnology, Technical University of Denmark, DTU-Building 345 East, DK-2800 Kongens Lyngby, Denmark

e-mail: mads.brandbyge@nanotech.dtu.dk

presented. Among the possible uses of the interface, the effects on the predicted signal of pH, buffer ionic strength, analyte concentration, and analyte relative orientation on nanowire surface are illustrated. Wherever possible, a comparison to experimental data available in literature is given, displaying the potential of BioFET-SIM for interpreting experimental results.

List of Abbreviations and Symbols

FET	Field Effect Transistor
r_{nw}	Nanowire radius
r_{ox}	Oxide layer thickness
r_{bf}	Biofunctionalization layer thickness
ϵ	Free space permittivity
ϵ_1	Nanowire permittivity
ϵ_2	Oxide permittivity
ϵ_3	Buffer permittivity
μ	Nanowire charge carrier mobility
n_0/p_0	Nanowire (electron/hole) charge carrier density
λ_{TF}	Nanowire Thomas–Fermi screening length
λ_{D}	Buffer Debye screening length
e	Unit of charge
\hbar	Plank’s constant divided by 2π
m^*	Charge carrier effective mass
k_{B}	Boltzmann’s constant
N_{A}	Avogadro’s number

3.1 Introduction

Nanowire-based field effect transistor (FET) biosensors have recently been the subject of much research and development. A *sensor* is a device that permits the recognition of an analyte in a sample through some form of interaction and the generation of a signal that can be recorded. According to [1] a *biosensor* is “a self-contained integrated device, which is capable of providing specific quantitative or semi-quantitative analytical information using a biological recognition element (biochemical receptor) which is retained in direct spatial contact with an electrochemical transduction element.” Nanoscale materials offer a large surface-to-bulk ratio and thus a high sensitivity towards changes in the charge distribution near the surface and are thus highly interesting for sensing. *Nanobiosensors* are characterized by a transduction element of nanoscale dimensions, like nanotubes, nanoribbons, or nanowires. The latter is the subject of this chapter.

Nanowire-based biosensors work as FETs: the current flowing through the semi-conducting nanowire material is perturbed by the sensing event involving a charge

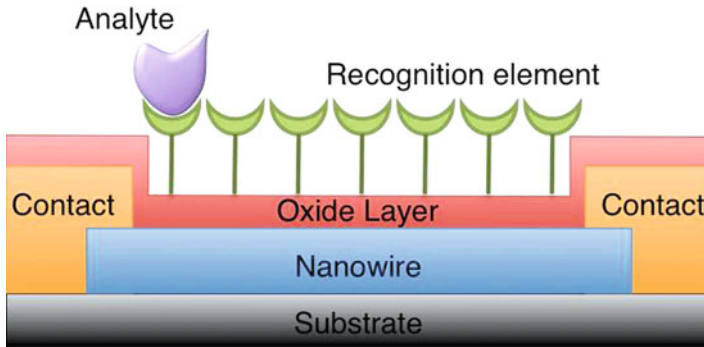


Fig. 3.1 Generic representation of a biofet. An insulating substrate carries a nanowire (transduction element) contacted at its extremes. An oxide layer is deposited on top. Biochemical receptors are chemically bond to form the recognition element capable of specifically recognizing the desired analyte

redistribution at the surface of the nanowire. Generally with an n -type nanowire a positive surface charge produces a positive signal (i.e., higher conductance) and *vice versa*. The opposite is true for a p -type nanowire. In an n -type (p -type) nanowire the charge carriers are electrons (holes). The change in surface potential created by a charge attracts or repels the charge carriers, creating the change in conductance. In a nanowire-based biosensor (for simplicity only called biofet from now on) a nanowire resides on an insulating substrate and is electrically contacted at its extremes, Fig. 3.1. Usually a second insulating layer, commonly constituted by an oxide, is deposited on top. Finally the analyte recognition layer is created through chemical modifications of the surface. The latter layer contains the recognition element and is responsible for specific capturing of the desired analyte and is usually referred to as a biofunctionalization layer. Examples of a biofunctionalization layer are a biotinylated surface for sensing of avidin or streptavidin [2, 3], or an antibody modified surface for the recognition of a given antigen [4].

Biofets have been employed or studied for pH [5], protein [3, 6–8], and DNA sensing [9, 10], for blood analysis [11] and for applications in nanotechnology-based medicine [12]. See [13–17] for a more thorough review of biofets and [18–20] for studies on their performance limits.

In addition to the experimental work, a series of numerical theoretical models have been presented to evaluate the performance of biofets [21–27]. Based on this theoretical work, tools for simulating biofets have been made available [28–30]. Following the work of Sørensen et al. [31] we developed our own model for simulation of the conductance sensitivity of a biofet in the presence of an analyte represented by a single charge [32]. We named our model BioFET-SIM. Section 3.2 gives a description of the theoretical background of BioFET-SIM and the approximations involved. BioFET-SIM has been subsequently extended to simulate the signal given by multiple charges approaching the surface of a biofet [33]. The usage of a multiple charges model proved essential when simulating the capture

of analytes with an asymmetric charge distribution. Recently BioFET-SIM has been further extended [34] to include explicitly the biofunctionalization layer and made available through a web interface hosted at www.biofetsim.org. The main advantage of the web interface is the possibility to graphically interact with the sensed analyte, in order to define the specific orientation of it with respect to the nanowire surface. Further details on the usage of BioFET-SIM are given in Sect. 3.3 and some possible applications are shown in Sect. 3.4. Thanks to its simplicity of use BioFET-SIM is a tool successfully employed in present day research [4, 35–42].

3.2 Theoretical Background

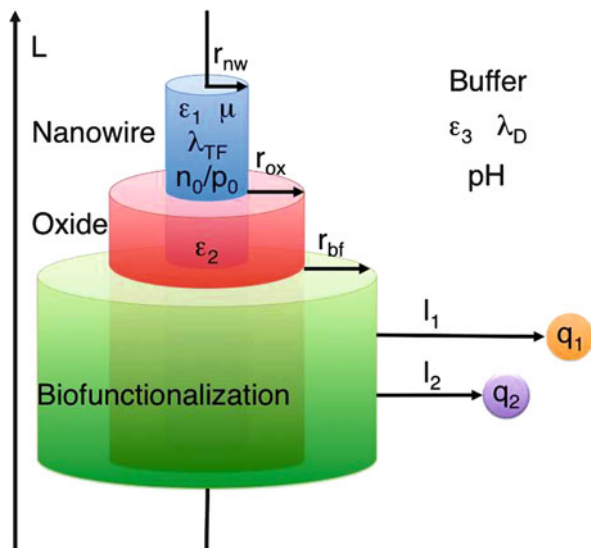
In this section we will review equations and assumptions behind the BioFET-SIM model.

3.2.1 Base Conductance

The BioFET-SIM model describes nanowire-based biosensors with elements as depicted in Fig. 3.2. The BioFET-SIM model predicts the conductance sensitivity $\Delta G/G_0$ where ΔG is the difference between the conductance upon binding, G , and the base conductance, G_0 , of the nanowire. The bulk conductance G_0 of a homogeneous cylindrical nanowire can be expressed as:

$$G_0 = \frac{\pi r_{nw}^2 e (n_0 \mu_n + p_0 \mu_p)}{L} \tag{3.1}$$

Fig. 3.2 Graphical representation of a generic nano BioFET. A nanowire of length L and radius r_{nw} is coated with an oxide layer of thickness r_{ox} . On the surface a biofunctionalization layer of thickness r_{bf} is responsible for capturing the analyte, represented by the charges q . The entire system is immersed in a buffer solution



where r_{nw} is the radius of the wire, e the elementary charge, n_0 the electron density, μ_n the electron mobility, p_0 the hole density, μ_p the hole mobility, and L the length of the nanowire. For a nanowire material with high enough doping, (3.1) can be approximated by considering only the electron or the hole density (only n_0 or p_0) and mobility (indicated simply as μ). For example, for a doped p -type nanowire, it is possible to rewrite (3.1) as:

$$G_0 = \frac{\pi r_{\text{nw}}^2 e p_0 \mu}{L} \quad (3.2)$$

In our model only one type of charge carrier for the entire nanowire is considered, and the nanowire is assumed to resemble a low density material. $\Delta G/G_0$ is evaluated through a Thomas–Fermi screening model of the charge carriers [43–45].

A major assumption governs the description of the charge carrier concentration, that is the charge carrier concentration is distributed uniformly through the nanowire. This implies that effects of, e.g., charges trapped in the oxide layer are not considered as influencing the charge carrier distribution. One has to remember that, formally, n_0 (p_0) represents the initial charge carrier density.

Moreover, we assume here that effects related to the metal contacts are negligible.

3.2.2 Conductance Sensitivity

Following [31] one can define the generic sensitivity of a p -type doped nanowire as:

$$\frac{\Delta G}{G_0} = - \frac{2}{r_{\text{nw}} e p_0} \Gamma \sigma_s \quad (3.3)$$

where σ_s is the “sensed” charge density at the surface of the nanowire and Γ is a dimensionless function quantifying the actual sensitivity of the nanowire. In case of an n -type nanowire (3.3) becomes:

$$\frac{\Delta G}{G_0} = \frac{2}{r_{\text{nw}} e n_0} \Gamma \sigma_s \quad (3.4)$$

In the special case of a cylindrical nanowire it is possible to express Γ analytically as [46]:

$$\Gamma = \frac{\varepsilon_1 K_0 \left(\frac{r_{\text{nw}} + r_{\text{ox}}}{\lambda_D} \right) \frac{\lambda_D}{\lambda_{\text{TF}}} I_1 \left(\frac{r_{\text{nw}}}{\lambda_{\text{TF}}} \right)}{\left[K_0 \left(\frac{r_{\text{nw}} + r_{\text{ox}}}{\lambda_D} \right) \left(\frac{\lambda_D}{r_{\text{nw}} + r_{\text{ox}}} \right) + \ln \left(\frac{r_{\text{nw}} + r_{\text{ox}}}{r_{\text{nw}}} \right) K_1 \left(\frac{r_{\text{nw}} + r_{\text{ox}}}{\lambda_D} \right) \frac{\varepsilon_3}{\varepsilon_2} \right] \varepsilon_1 \left(\frac{r_{\text{nw}}}{\lambda_{\text{TF}}} \right) I_1 \left(\frac{r_{\text{nw}}}{\lambda_{\text{TF}}} \right) + \varepsilon_3 K_1 \left(\frac{r_{\text{nw}} + r_{\text{ox}}}{\lambda_D} \right) I_0 \left(\frac{r_{\text{nw}}}{\lambda_{\text{TF}}} \right)} \quad (3.5)$$

where λ_D is the Debye screening length of the buffer, λ_{TF} the Thomas–Fermi screening length typical of the nanowire material, ε_1 , ε_2 , and ε_3 are the relative

permittivities of the nanowire, the oxide layer, and the buffer, respectively, r_{ox} is the oxide layer thickness, I_0 , I_1 , K_0 and K_1 are the modified Bessel functions of first and second kind, respectively [47]. Γ is a dimensionless function with values ranging from zero to unity.

3.2.3 Single Charge Model

The presence of additional charges at a distance l from the nanowire surface gives rise to a charge density σ_b . Equation (3.3) is rewritten as:

$$\frac{\Delta G}{G_0} = -\frac{2}{r_{\text{nw}} e p_0} \Gamma (\Gamma_l \sigma_b + \sigma_s) \quad (3.6)$$

The BioFET-SIM model concerns the simulation of a signal in the conductance when an analyte is attached to the surface. The analyte is represented by σ_b and it is supposed not to modify the charge density σ_s already present at the nanowire surface. The conductance given by σ_s is considered as part of the background signal. For this reason the σ_s term can be dropped from (3.6) that can be written as:

$$\frac{\Delta G}{G_0} = -\frac{2}{r_{\text{nw}} e p_0} \Gamma (\Gamma_l \sigma_b) \quad (3.7)$$

and Γ_l is defined as:

$$\Gamma_l = 2 \frac{r_{\text{nw}}}{r_{\text{nw}} + l} \left(1 + \sqrt{\frac{r_{\text{nw}}}{r_{\text{nw}} + l}} \exp(l/\lambda_D) \right)^{-1} \quad (3.8)$$

where l is the distance of the sensed charge from the nanowire surface, inclusive of the biofunctionalization layer (r_{bf}). If the analyte is approximated as one charge as in Fig. 3.3a, (3.5), (3.7), and (3.8) describe the single charge BioFET-SIM model [32].

3.2.4 Multiple Charges Model

A complex analyte system like a protein can give rise to unexpected signals because of its nonuniform charge distribution [48]. In these cases a single charge description of the sensing event is not sufficient. Considering multiple charges, the sensitivity is evaluated as:

$$\frac{\Delta G}{G_0} = -\frac{2}{r_{\text{nw}} e p_0} \Gamma \left[\sum_i^m (\Gamma_{i,\text{tot}} \sigma_{b_i}) \right] \quad (3.9)$$

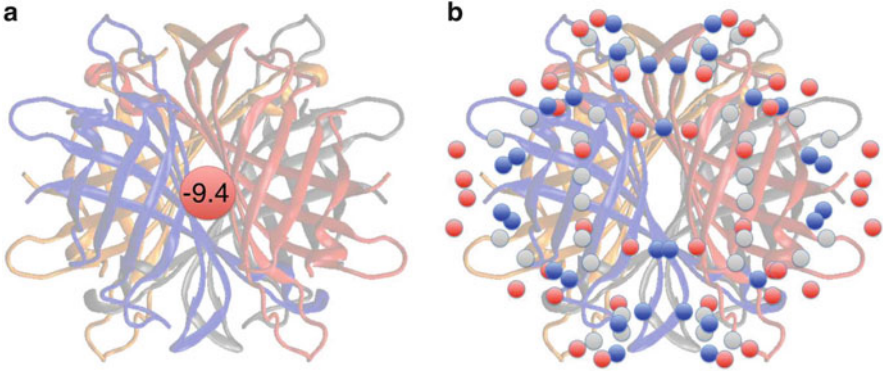


Fig. 3.3 PROPKA computed charges at $\text{pH} = 7.4$ for streptavidin (see Sect. 3.2.8). (a) The overall charge is assumed to reside at the center of mass of the protein (single charge model). (b) Each ionizable amino acid carries its charge (multiple charges model). Blue, white, and red circles correspond to a positive, neutral, and negative charge, respectively

and $\Gamma_{i,\text{tot}}$ is defined as:

$$\Gamma_{i,\text{tot}}(\lambda_D) = 2 \frac{r_{\text{nw}}}{r_{\text{nw}} + l_{i,\text{tot}}} \left[1 + \sqrt{\frac{r_{\text{nw}}}{r_{\text{nw}} + l_{i,\text{tot}}} e^{l_{i,\text{tot}}/\lambda_D}} \right]^{-1} \quad (3.10)$$

where $l_{i,\text{tot}}$ is the overall distance of the charge q_i from the surface of the nanowire. Considering Fig. 3.2, the distance $l_{1,\text{tot}}$ relative to q_1 is computed as:

$$l_{1,\text{tot}} = r_{\text{ox}} + r_{\text{bf}} + l_1 \quad (3.11)$$

Equations (3.5), (3.9), and (3.10) constitute the multiple charges BioFET-SIM model [33]. Figure 3.3b reports the multiple charges description of streptavidin. Each blue, white, and red circles represents a positive, neutral, and negative q_i charge, respectively. A more detailed description of how BioFET-SIM computes $l_{i,\text{tot}}$ is given in [34].

Note that we approximate the charge distributions of the charges as homogeneous over the nanowire surface, and only varying outwards perpendicular to the nanowire surface. This approximation enables analytical solutions, very fast calculations, and high-throughput simulations.

3.2.5 Thomas–Fermi Screening Length

In the BioFET-SIM model we settle on a rough description of the electronic structure in the nanowire reflecting our lack of detailed knowledge about the complex situation at its surface. The possible deactivation of dopants at the surface [49] or the increased dopant concentration near the surface compared to the semiconductor

bulk [50] is approximated by the sole Thomas–Fermi screening length λ_{TF} [32]. For the p -type (n -type) nanowire, the screening length λ_{TF} is related to the charge carrier density p_0 (n_0) through:

$$\lambda_{\text{TF}} = \sqrt{\frac{\hbar^2 \varepsilon_r \pi^{4/3}}{m^* e^2 p_0^{1/3}}} \quad (3.12)$$

where ε_r is the relative permittivity of the nanowire material ($\varepsilon_0 \varepsilon_1$) and m^* is the effective mass of the charge carrier in units of an electron mass at rest. p_0 would be replaced by n_0 for an n -type nanowire. Equation (3.12) states that λ_{TF} can be interpreted as a measure for the distance between charge carriers (related to the charge carrier density) in the nanowire under no applied bias. Therefore this parameter can be used to simulate the effect of the back gate in an experimental setup. The presented linearized model is not capable of describing nonlinear effects such as inversion mode of operation. However, the model distinguishes between accumulation/depletion mode of operation by allowing to choose between an n - or p -type material and different values of λ_{TF} .

3.2.6 Debye Screening Length

Buffer characteristics influence device performance, as described for experimental [39, 51, 52] and predicted [32] conductance signals. The screening of the analyte signal by the electrolyte is implemented through (3.8) and (3.10), which depend on the Debye length:

$$\lambda_{\text{D}} = \sqrt{\frac{\varepsilon_0 \varepsilon_3 k_{\text{B}} T}{2 N_{\text{A}} e^2 I}} \quad (3.13)$$

where ε_0 is the free space dielectric constant, K is the Boltzmann constant, T is the absolute temperature of the experiment, N_{A} is Avogadro's number, and I is the ionic strength of the solution. The expression for the ionic strength is given by:

$$I = 1/2 \sum_i c_i z_i^2 \quad (3.14)$$

where c_i indicates the concentration of ion species i and z_i is its formal charge.

This description of the electrolyte assumes that (a) the electrolyte is in equilibrium, i.e. the chemical potential is at a minimum and (b) the value for λ_{D} used in (3.8) and (3.10) is equal to the Debye length of the bulk buffer. We note that in principle these values can differ due to the biofunctionalization layer [31].

3.2.7 Biofunctionalization Layer

The biofunctionalization layer represents the chemical modifications to the nanowire surface, enabling it to capture the desired analyte. It can be visualized as a forest of linker molecules, Fig. 3.1. These molecules are not densely packed and are supposed to be immersed in the buffer solution. For this reason the biofunctionalization layer is implemented solely as a distance parameter, providing a measure of the spatial extension of the linker molecules. If the linker molecules would be so densely packed to exclude the buffer, an extra dielectric constant would be necessary to describe the effect of the biofunctionalization layer on the signal. Charges on the linker molecules are not considered influencing the signal, but part of the background conductance, see Sect. 3.2.3. In principle the surface functionality of the nanowire is not uniform [6] and requires a combined description of the pH-dependent charge on the linker molecules as well as the oxide where a common description of the charge of the oxide layer is through the site-binding model [53].

3.2.8 Protein Charges

The coverage of the biofet with analyte is described in Sect. 3.3.2. A common usage for biofets is the sensing of proteins [3, 6–8]. BioFET-SIM is specifically tailored for this. The PROPKA method [54–56] is employed to compute the pK_a values of each ionizable amino acid of a given protein structure. The computed pK_a values are used to evaluate the protonation state (charge) of each ionizable residue i as a function of pH as:

$$q_i(\text{pH}) = \frac{10^{pK_a^i - \text{pH}}}{1 + 10^{pK_a^i - \text{pH}}} - p(i) \quad (3.15)$$

where $p(i) = 1$ for $i \in \{\text{Asp, Glu, C-, Tyr, Cys}\}$ and $p(i) = 0$ otherwise. In (3.15), $q_i(\text{pH})$ is the probability for the amino acid to be protonated [57]. In the single charge model (Sect. 3.2.3) the computed charges are summed together and a single charge is placed at the center of mass of the protein (Fig. 3.3a). In the multiple charges model (Sect. 3.2.4) a three-dimensional charge distribution is obtained by placing the charge computed with (3.15) at the average of the coordinates of the terminal atoms of the side chain of residue i (Fig. 3.3b). It is assumed that protein binding to the nanowire does not affect the pK_a values computed by PROPKA, nor disrupt the overall protein conformation.

3.2.9 Summary

To summarize, the BioFET-SIM model evaluates the conductance sensitivity signal $\Delta G/G_0$ (Sect. 3.2.2) of a biofet as depicted in Fig. 3.2. The model considers a

nanowire of length L and radius r_{nw} and described through its permittivity (ϵ_1), mobility (μ), charge carrier density (n_0/p_0), and Thomas–Fermi screening length (λ_{TF} , Sect. 3.2.5). The nanowire is coated with an oxide layer of thickness r_{ox} and characterized by permittivity ϵ_2 . On top of the oxide layer a biofunctionalization layer (Sect. 3.2.7) of thickness r_{bf} is responsible for capturing the desired analyte. The analyte charges are evaluated according to the buffer pH (Sect. 3.2.8) and placed at a certain distance l from the nanowire. The conductance sensitivity is evaluated with the analyte charges or summed in a single charge (Sect. 3.2.3) or separate (Sect. 3.2.4). The entire system is immersed in a buffer solution described by the Debye screening length (λ_{D} , Sect. 3.2.6) and its permittivity (ϵ_3).

3.3 Usage

The BioFET-SIM method is available as a graphical web interface at the address www.biofetsim.org where a link to an [instruction video](#) to its usage is present. BioFET-SIM is distributed as open source through GitHub, and links to the [source code](#) as well as to the [command line version](#) of the program are also present on the web interface page. The web interface appears as shown in Fig. 3.4. A detailed description of the web interface and how to use it, along with a description of the uses of the command line version, are given in [34]. The following sections give a brief description of the interface and how the number of sensed analyte is computed. In the last section a simple example of the interface usage is given.

3.3.1 Interface Usage

The upper part of the web interface permits the selection of the protein structure that will act as analyte. The structure can be simply defined through its PDB identifier, to be downloaded from the PDB database (www.pdb.org [58]), or uploaded in PDB format. A pH value for the charges evaluation (Sect. 3.2.8) is also inserted, with default value 7.4.

By initializing the interface, the chosen structure is displayed over a representation of the nanowire surface. In the interface it is possible to regulate the relative orientation of the protein structure to the surface.

In the lower part of the interface it is possible to define all the various parameters needed to characterize the biofet, as previously described in Sects. 3.2.1–3.2.7. The interface permits also to define the number of sensed analyte molecules, as described in Sect. 3.3.2.

Upon performing a BioFET-SIM calculation, the computed value for the sensitivity is displayed, along with a graph showing the change in sensitivity against

BioFET-SIM Online

www.biofetsim.org

BioFET-SIM 2.0

BioFET-SIM 1.0 (Mobile friendly), Recommended values

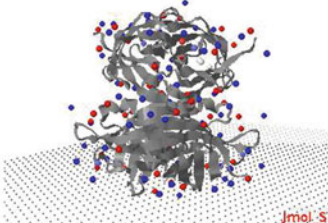
Upload a file: No file selected. File requirements

OR

Download from PDB: pH Value:

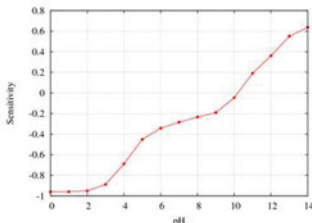
Use uploaded:
(Enable when using an uploaded structure)

Ready.



Jmol JS

Use Alt-left (Alt-right on Linux) and drag the structure to adjust the orientation.



Structure: 1AVD

Q_{ot} at pH 7.4: 16.59 [e]
Base conductance G_0 : 279.3529
Sensitivity: -0.2608

NW Properties	Value	Lower Limit	Upper Limit	Plot
NW Length [nm]:	<input type="text" value="2000.0"/>	<input type="text" value="1500.0"/>	<input type="text" value="2500.0"/>	<input type="radio"/>
NW Radius [nm]:	<input type="text" value="10.0"/>	<input type="text" value="8.0"/>	<input type="text" value="12.0"/>	<input type="radio"/>
Thomas-Fermi Length [nm]:	<input type="text" value="2.04"/>			
NW Permittivity [ϵ_0]:	<input type="text" value="12.0"/>			
Charge Carrier Mobility [$m^2V^{-1}s^{-1}$]:	<input type="text" value="0.01"/>			
Charge Carrier Density [m^{-3}]:	<input type="text" value="1.11e+24"/>			
NW Type:	<input checked="" type="radio"/> p-type			<input type="radio"/> n-type
Oxide and Biofunctionalization Layer Properties				
Oxide Layer Thickness [nm]:	<input type="text" value="2.0"/>	<input type="text" value="1.0"/>	<input type="text" value="3.0"/>	<input type="radio"/>
Oxide Layer Permittivity [ϵ_0]:	<input type="text" value="3.9"/>			
Biofunctionalization Thickness [nm]:	<input type="text" value="1.0"/>			
Solvent Properties				
Debye Length [nm]:	<input type="text" value="2.0"/>	<input type="text" value="1.0"/>	<input type="text" value="3.0"/>	<input checked="" type="radio"/>
Solvent Permittivity [ϵ_0]:	<input type="text" value="78.0"/>			
Calculation				
Charge Model:	<input type="radio"/> Single			<input checked="" type="radio"/> Multiple
Number of Proteins on NW:	<input type="text" value="4000"/>			<input checked="" type="checkbox"/> Constant?

Fig. 3.4 BioFET-SIM web interface at www.biofetsim.org. The screenshot shows the interface being used to simulate the pH response to the sensing of 4,000 avidin proteins using default nanowire values

a chosen simulation parameter. An example is given in Sect. 3.3.3. Through the interface it is possible to save a state file which records the chosen relative orientation of the protein and the nanowire surface and an input file for the command line version of the program. The command line version is a powerful tool that allows the user to reproduce a calculation as well as performing many similar ones changing only one parameter at the time.

3.3.2 *Analyte Surface Coverage*

In order to apply (3.7) or (3.9) the sensed charge density σ_b has to be defined. Once defined the geometry of the nanowire, the charge density can be retrieved from the number of sensed analyte molecules. The web interface has two possible options for inserting the number of sensed molecules: full coverage or user specified.

The full coverage option assumes that the analyte molecules are perfectly packed in order to completely fill the available surface of the biofunctionalization layer. Full coverage of the nanowire has been demonstrated experimentally [59]. Once the relative orientation of the protein to the surface is defined, the interface computes the area on the surface occupied by the molecule. The surface of the biofunctionalization layer is then divided by this area to compute the number of sensed proteins. See [34] for further details.

The user can also specify a fixed number of bound proteins. This can be used, e.g., when it is known that the number of linker molecules on the biofet surface remains constant, even if the proteins bind with different orientations.

It is important to note that this treatment of the protein—biofunctionalization binding assumes that all proteins bind with the same orientation to the surface.

3.3.3 *Example: Sensitivity Dependence on Oxide Layer Thickness*

In this section we show the basic usage of BioFET-SIM to simulate the effects of different thickness values of the oxide layer. The simulation uses the default values for a p -type doped silicon nanowire as found on the web interface and reported in Table 3.1. The conductance sensitivity is evaluated for the sensing of 4,000 avidin proteins (PDB identifier 1AVD) at pH 7.4 and the single charge model.

The computed sensitivity is reported in Fig. 3.5. Avidin carries a positive charge and induces a negative signal on the p -type doped nanowire. As expected, to a thicker oxide layer corresponds a diminished (in absolute value) sensitivity. The web interface permits to obtain the plot of Fig. 3.5 with a few simple clicks.

Table 3.1 Parameters defining the simulated biofet

Parameter	Symbol	Value	(Units)
Nanowire length	L	2,000.0	(nm)
Nanowire radius	r_{nw}	10.0	(nm)
Thomas–Fermi length	λ_{TF}	2.04	(nm)
Charge carrier density	p_0	1.11×10^{24}	(m^{-3})
Charge carrier mobility	μ	0.01	($m^2 V^{-1} s^{-1}$)
Nanowire permittivity	ϵ_1	12.0	(ϵ_0)
Oxide layer thickness	r_{ox}	2.0	(nm)
Oxide layer permittivity	ϵ_2	3.9	(ϵ_0)
Biofunctionalization layer thickness	r_{bf}	1.0	(nm)
Solvent permittivity	ϵ_3	78.0	(ϵ_0)
Buffer Debye length	λ_D	2.0	(nm)

We simulate the nanowire as being silicon p -type doped

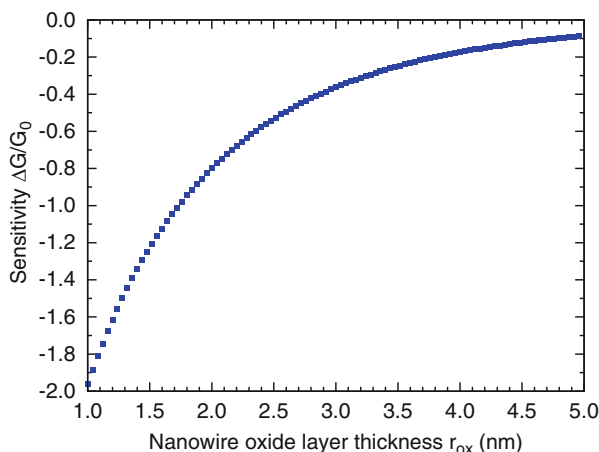


Fig. 3.5 Computed sensitivity response to the sensing of 4,000 molecules of avidin when changing the oxide layer thickness from 1.0 to 5.0 nm

3.4 Applications

The following sections illustrate some of the possible applications of BioFET-SIM. Whenever possible, the computed results are compared to experimental results.

3.4.1 Single Charge Model

For some applications the simpler single charge model (Sect. 3.2.3) is sufficient. In particular the sensing of avidin (PDB identifier 1AVD [60]) or streptavidin (PDB identifier 1STP [61]) is nearly independent from the used model. See Fig. 4

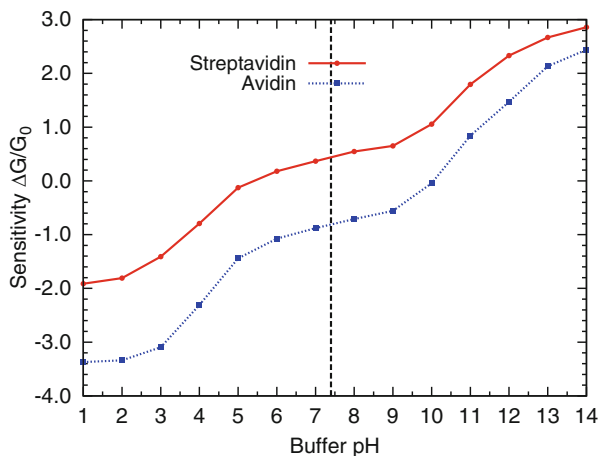


Fig. 3.6 Computed sensitivity response to the sensing of 4,000 molecules of avidin (*dotted line*, square points) or streptavidin (*full line*, round points) on a biotinylated surface with the single charge model. Dependence of the signal on the buffer pH

of [33]. In fact these two proteins are quite symmetrical and do not present any orientation that would favor one type of charges over the other. Another situation when the single charge model is required is represented by the binding of proteins with random orientations (i.e., generic adsorption) over the biofet surface. Random orientations average the protein charge distribution to the protein overall charge.

3.4.1.1 Effect of pH on Signal

At a pH value of 7.4 (physiological pH) avidin and streptavidin have opposite charge. This difference was exploited in [3], where the two proteins could be discerned by their opposite signal. The computed difference in signal for the sensing of avidin and streptavidin is illustrated in Fig. 3.6. At pH 7.4 (vertical dashed line) PROPKA computes a charge of 16.6 and $-9.4 e$ for avidin and streptavidin, respectively (Sect. 3.2.8). This results in a positive signal for streptavidin and a negative signal for avidin.

In the same experiment [3] Stern et al. recorded also the change in signal at different pH values when sensing avidin. Figure 3.6 (dotted line) shows how the expected signal changes with different pH. At low pH values a negative signal is expected. At pH values around 10 the predicted signal is close to zero, while at higher pH values it is possible to obtain a positive signal. Obviously, this simulation does not consider the possible effects of very acid or very basic environments on the structure of the protein [39].

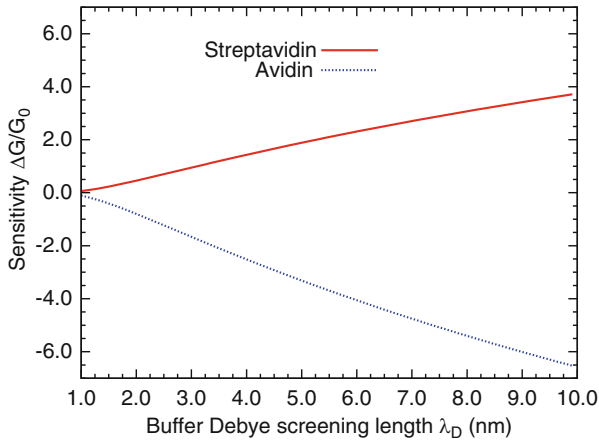


Fig. 3.7 Computed sensitivity response to the sensing of 4,000 molecules of avidin (*dotted line*, square points) or streptavidin (*full line*, round points) on a biotinylated surface with the single charge model. Dependence of the signal on the buffer Debye screening length

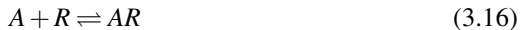
3.4.1.2 Signal Dependence on the Debye Screening Length

The intensity of a signal depends also on the ionic strength of the employed buffer solution. At short Debye lengths (high ionic strength, Sect. 3.2.6) a small signal is expected. In [51] Stern et al. analyze the dependence of signal upon dilution of buffer. Figure 3.7 depicts the BioFET-SIM evaluated signal for different Debye lengths for avidin and streptavidin at pH 7.4. It is evident that at longer Debye lengths the difference between the two proteins signals is more and more accentuated. A more complex example on how to use the signal dependence on λ_D to extrapolate information on the system can be found in [4, 34] and in Sect. 3.4.3 (Fig. 3.11).

3.4.1.3 Signal Dependence on Analyte Concentration

Stern et al. in [3] also analyze how the signal changes for different concentrations of analyte streptavidin. The dependence of the number of captured analyte molecules on the bulk analyte concentration is needed to evaluate the corresponding signal. We present here a simple model to evaluate it. A more complex model can be found in [19], but the qualitative results are equivalent. We note that the values used by Nair et al. for the forward and reverse reaction constants in [18, 19] are typical for the binding of single strand DNA but not necessarily for (strept)avidin–biotin complexes.

In the following we consider the sensing reaction as at its equilibrium. The generic sensing of streptavidin on a biotinylated surface can be expressed as:



where A is the analyte (streptavidin), R the receptor and AR the complex. The equilibrium constant K , inverse of the dissociation constant K_D , is given by:

$$K = \frac{[AR]}{[A][R]} \quad (3.17)$$

For the streptavidin–biotin complex a dissociation constant $K_D = 4 \times 10^{-14} \text{ M}$ has been found [62] and consequently $K = 1/K_D = 2.5 \times 10^{13} \text{ M}^{-1}$.

The concentration of free analyte $[A]$ in equilibrium with the complex $[AR]$ with respect to the starting concentration of the added sample $[A_{\text{tot}}]$ is simply expressed by:

$$[A] = [A_{\text{tot}}] - [AR] \quad (3.18)$$

and similarly for the number of free receptors:

$$[R] = [R_{\text{tot}}] - [AR] \quad (3.19)$$

Inserting (3.18) and (3.19) in (3.17):

$$K = \frac{[AR]}{([A_{\text{tot}}] - [AR])([R_{\text{tot}}] - [AR])} \quad (3.20)$$

and using the substitutions $m = 1 + K([A_{\text{tot}}] + [R_{\text{tot}}])$ and $K' = K[A_{\text{tot}}][R_{\text{tot}}]$ it is possible to write the equation:

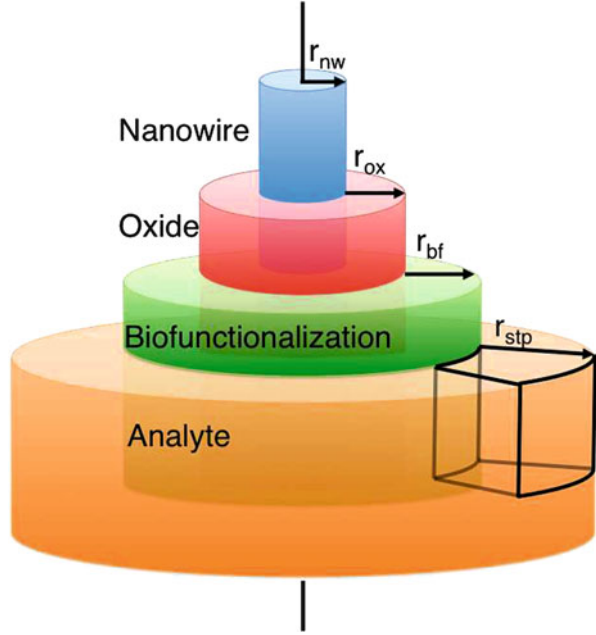
$$K[AR]^2 - m[AR] + K' = 0 \quad (3.21)$$

with solutions

$$\begin{aligned} [AR] &= \frac{1}{2K} \left(m + \sqrt{m^2 - 4KK'} \right) \\ &= \frac{1}{2K} \left(m - \sqrt{m^2 - 4KK'} \right) \end{aligned} \quad (3.22)$$

of which only the solution with the minus sign is significant (the other one giving $[AR] > [R_{\text{tot}}]$, which is not possible). Equation (3.22) defines the concentration of analyte-receptor complexes given the starting concentration of analyte in the sample $[A_{\text{tot}}]$, the concentration of initial receptor molecules $[R_{\text{tot}}]$, and the equilibrium constant K .

Fig. 3.8 Graphical representation of a generic nano BioFET sensing streptavidin. Supposing full coverage, the analyte creates a layer around the nanowire with thickness r_{stp} . Each streptavidin molecule occupies one cuboid as illustrated



BioFET-SIM requires the number of conjugated molecules, that is the number of formed complexes. This number can be obtained as:

$$n_{AR} = [AR] V_{\text{rec}} N_A \quad (3.23)$$

where V_{rec} is the total volume occupied by the conjugated analyte-receptor molecules. Supposing complete coverage by streptavidin molecules, the total volume V_{rec} occupied by the sensed molecules can be visualized as the outer shell in Fig. 3.8. The analyte occupied layer is supposed to be as thick as the analyte molecule itself (r_{stp}). The occupied volume can be computed as difference between the outer and inner volumes:

$$\begin{aligned} V_{\text{out}} &= \pi (r_{\text{nw}} + r_{\text{ox}} + r_{\text{bf}} + r_{\text{stp}})^2 L \\ V_{\text{in}} &= \pi (r_{\text{nw}} + r_{\text{ox}} + r_{\text{bf}})^2 L \\ V_{\text{rec}} &= V_{\text{out}} - V_{\text{in}} \\ &= \pi r_{\text{stp}} [2(r_{\text{nw}} + r_{\text{ox}} + r_{\text{bf}}) + r_{\text{stp}}] L \end{aligned} \quad (3.24)$$

Alternatively, supposing that each streptavidin molecule occupies a cube of volume r_{stp}^3 , as shown in Fig. 3.8, it is possible to express V_{rec} as:

$$V_{\text{rec}} = n_{R_{\text{tot}}} r_{\text{stp}}^3 \quad (3.25)$$

Table 3.2 Parameters used to simulate the sensing of streptavidin (1STP) depending on the analyte concentration

Parameter	Symbol	Value	(Units)
Analyte structure		1STP	
Charge at pH 7.4	q	-9.4	(e)
Bounding box side	r_{stp}	5.0	(nm)
Equilibrium constant	K	2.5×10^{13}	(M ⁻¹) ^a
Total number of receptors concentration	$[R_{\text{tot}}]$	0.013.3	(M) ^b
Volume occupied by the complex	V_{rec}	9.74×10^{-19}	(dm ³) ^c

^aComputed as $1/K_D$ where $K_D = 4 \times 10^{-14}$ from [62]

^bFrom (3.26)

^cFrom (3.24)

where $n_{R_{\text{tot}}}$ is the total number of effective receptor molecules. Using (3.25) it is possible to define $[R_{\text{tot}}]$ as:

$$\begin{aligned}
 [R_{\text{tot}}] &= \frac{n_{R_{\text{tot}}}/N_A}{V_{\text{rec}}} \\
 &= \frac{n_{R_{\text{tot}}}/N_A}{n_{R_{\text{tot}}} r_{\text{stp}}^3} \\
 &= \frac{1}{r_{\text{stp}}^3 N_A}
 \end{aligned} \tag{3.26}$$

The value obtained with (3.26) and the literature value for K are inserted in (3.22). The concentration of sensed molecules $[AR]$ is so defined as a function of the starting sample analyte concentration $[A_{\text{tot}}]$. $[AR]$ is inserted in (3.23) together with the value obtained with (3.24), to finally obtain the number of sensed analyte molecules n_{AR} to be used as input for BioFET-SIM.

The simulation was performed using the default values of BioFET-SIM (Table 3.1) together with those reported in Table 3.2. The obtained values for the sensitivity are reported in Table 3.3 and plotted in Fig. 3.9. Given experimental conditions as those reported in Tables 3.1 and 3.3, the simulation states that it is possible to expect a quasi-linear behavior in a concentration range 1–10 mM and a sensitivity limit of 0.1 mM. A different setup would be necessary in order to sense smaller concentrations of analyte, e.g. a larger nanowire radius to increase the number of captured molecules. Since sensitivity is inversely proportional to the nanowire radius [32], possibly a longer Thomas–Fermi screening length would be necessary to balance out the effects on sensitivity. It is important to remember that there are many simplifications behind the data of Table 3.3, but the qualitative result of Fig. 3.9 is anyway reliable. Further details can be found in [63].

Table 3.3 Streptavidin sensing simulation data

$[A_{\text{tot}}]$ (M)	n_{AR}	$\Delta G/G_0$
1.0×10^0	7,911	0.88584
1.0×10^{-1}	7,911	0.88584
1.2×10^{-2}	7,038	0.80022
1.0×10^{-2}	5,864	0.66637
8.0×10^{-3}	4,692	0.53333
6.0×10^{-3}	3,519	0.40016
4.0×10^{-3}	2,346	0.26723
2.0×10^{-3}	1,173	0.13305
1.0×10^{-3}	586	0.06664
5.0×10^{-4}	293	0.03332
1.0×10^{-4}	58	0.00666
1.0×10^{-5}	6	0.00067
1.0×10^{-6}	1	0.00007

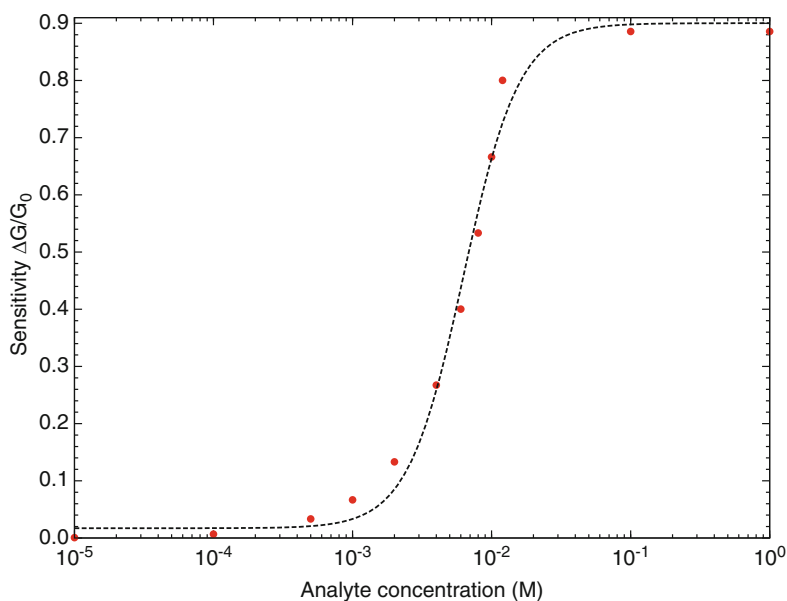


Fig. 3.9 Simulated signal response for the sensing of streptavidin in the concentration range 1×10^{-5} to 1 M with default BioFET-SIM settings. The *dots* correspond to the data of Table 3.3, while the *dashed lines* represent a sigmoid fit to guide the eye

3.4.2 Multiple Charges Model

When the sensed analyte has an asymmetric charge distribution, the single charge model is insufficient to describe its relative signal. However, since the underlying model is based on a linear equation it is possible to obtain the signal from distributions involving multiple charges as a sum of the individual responses.

In the following sections we show the importance of the multiple charges model (Sect. 3.2.4) through the sensing of a model peptide and a more complex example employing nucleocapsid protein.

3.4.2.1 Model Peptide Sensing

In this section we simulate the sensing of a model peptide constituted by two protonated lysine residues at the N-terminus, an eight alanine residues bridge and two deprotonated aspartic acid residues at the C-terminus: KK8ADD. The model was built as a linear peptide using PyMOL [64]. At pH 7.4 PROPKA computes a charge of $0.22 e$. The peptide has a clear asymmetric charges distribution: three positive charges at the N-terminus and three negative charges at the C-terminus and overall charge nearly zero. The single charge model would predict a nearly zero signal for the sensing of this peptide. If there was the possibility of a biofunctionalization layer capable of specifically capturing aspartic or lysine residues, it would be possible to selectively bind the peptide as represented in Fig. 3.10a, c, respectively. The corresponding simulated signal as function of the Debye screening length is shown in Fig. 3.10d. If otherwise the peptide would be simply adsorbed on the nanowire surface in a horizontal position, the expected signal would be nearly zero. The same zero signal would also be expected if the charges distribution would average out because of random capturing. In fact, in case of random capturing of the analyte no specific direction relative to the nanowire surface would be preferred. In this case the single charge model would be sufficient.

3.4.2.2 Nucleocapsid Protein Sensing

The sensing of nucleocapsid protein (N-protein), as performed by Ishikawa et al. [48], is presented in this section, to exemplify the potential of BioFET-SIM and the multiple charges model.

In their work Ishikawa and co-workers employed In_2O_3 *n*-type doped nanowire-based sensors. Table 3.4 reports the different from the default parameter values used to simulate such devices. At pH 7.4 PROPKA computes a charge of $6.4 e$ for N-protein. The sensing of this protein by an *n*-type doped nanowire-based sensor should produce a positive signal, but a negative one was recorded [48]. It is possible to use BioFET-SIM to investigate the possible causes of this unexpected signal.

N-protein has an asymmetric charge distribution, as shown in Fig. 3.11a, e in the case of pH = 7.4. The protein could be captured by the biofunctionalization layer as reported in Fig. 3.11a, where the bulk of the protein rich in negative charges is closer to the nanowire surface. We refer to this situation as *up*. It is also possible that the protein is captured as depicted in Fig. 3.11e, that is with the positive charges rich hairpin closer to the nanowire surface. We refer to this second possibility as *down*. The two possible orientations *up* and *down* would generate quite different signals at pH = 7.4, as depicted in Fig. 3.11c, g, respectively. In the *up* orientation a small

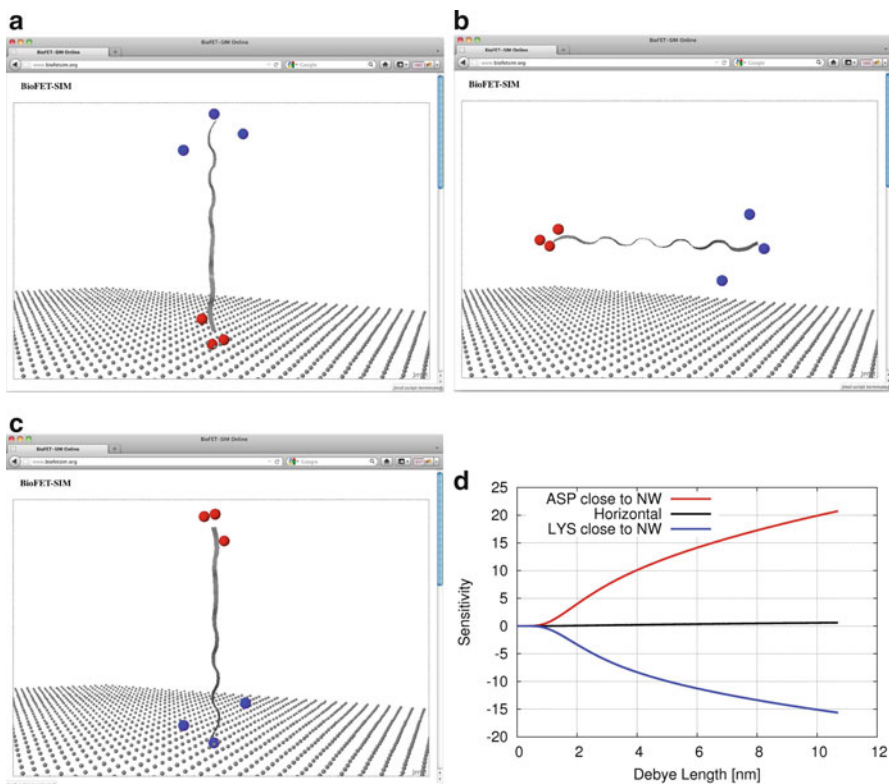


Fig. 3.10 Possible orientations and corresponding signal for the model peptide KK8ADD. The BioFET-SIM simulation was conducted with default values and the multiple charges model. The capturing of the peptide can be specific for (a) Asp or (c) Lys or (b) the peptide could be simply adsorbed horizontally on the surface. (d) The simulated signals as function of the Debye screening length for the different peptide—nanowire relative orientations. Figures originally from [34]: (a)–(c) [doi:10.1371/journal.pone.0045379.g004](https://doi.org/10.1371/journal.pone.0045379.g004), (d) [doi:10.1371/journal.pone.0045379.g005](https://doi.org/10.1371/journal.pone.0045379.g005)

negative signal is expected for Debye screening lengths up to 3 nm (Fig. 3.11c). In the *down* orientation a clear positive signal is expected at any buffer dilution (Fig. 3.11g).

Varying the pH of the buffer solution would change the expected signal. At pH = 3.8 N-protein has a computed charge of 22.3 e , ca. three times higher than at pH = 7.4. The protein is now mainly constituted by positive charges and both orientations produce similar positive signals (Fig. 3.11b, f). At pH = 11.0, instead, N-protein has a computed negative charge of $-3.2 e$. The predicted signal for the *up* orientation is clearly negative at any buffer dilution (Fig. 3.11d). For the *down* orientation a nearly zero but positive signal is predicted for Debye screening lengths from 1 to 3 nm (Fig. 3.11h). It is interesting to note that, by inverting the charge of

Table 3.4 Parameters defining the simulated In₂O₃ *n*-type semiconducting nanowire-based device that differs from those of Table 3.1

Parameter	Symbol	Value	(Units)
Nanowire radius	r_{nw}	5.0	(nm)
Oxide layer thickness	r_{ox}	0.0	(nm)
Thomas–Fermi length	λ_{TF}	1.179	(nm)
Charge carrier density	n_0	4.6×10^{25}	(m ⁻³)
Charge carrier mobility	μ	0.0078	(m ² V ⁻¹ s ⁻¹)
Nanowire permittivity	ϵ_1	9.0	(ϵ_0)

N-protein by changing the pH value from 7.4 to 11.0, also the expected signals for the *up* and *down* orientations are inverted.

The different simulated signals for the sensing of N-protein show that the BioFET-SIM model with multiple charges can be employed to study the possible effects of different orientations of the analyte with respect to the nanowire surface, coupled with the effects of different pH values of the buffer solution. In the specific case of N-protein we showed that, given certain conditions (e.g. Fig. 3.11c), an unexpected negative signal is possible.

3.4.3 Antigen Sensing on an Antibody Functionalized Surface

In this section we present a complex application of BioFET-SIM. Following [4], we decided to study the sensing of an antigen captured by an antibody functionalized biofet surface. Differences in the surface functionalization led to different signals, even if stemming from sensing the same antigen in otherwise similar conditions. This is indicative of different average distances between the sensed antigen and the biofet surface. Antibody binding to the surface was made possible through either an N-terminus located on the antigen-binding fragment (Fab) or by one or both C-termini at the antibody base, as shown in Fig. 3.12. N-terminus binding led to a reported antigen—surface distance of 5.9 ± 0.6 nm. C-termini binding corresponded to an antigen—surface distance of 8.4 ± 0.4 nm [4].

We decided to study the effect of possible antibody orientations on the signal. We further developed the formalism presented in Sect. 3.2 in order to obtain a quantity (the relative sensitivity factor) which depends solely on Debye length and distance of the sensed analyte from the surface. The derivation of this quantity is described in Sect. 3.4.3.1. Section 3.4.3.2 describes the necessary steps to prepare the antibody and antigen structures for the BioFET-SIM simulations. Section 3.4.3.3 shows the different orientations of the antibody, and consequently of the sensed antigen, over the biofet surface that we considered in this study. Finally, by performing a series of simulations at different Debye lengths, corresponding to those employed experimentally in [4], it was possible to obtain through a fit the average distance of the sensed antigen from the nanowire surface. These results are presented in Sect. 3.4.3.4.

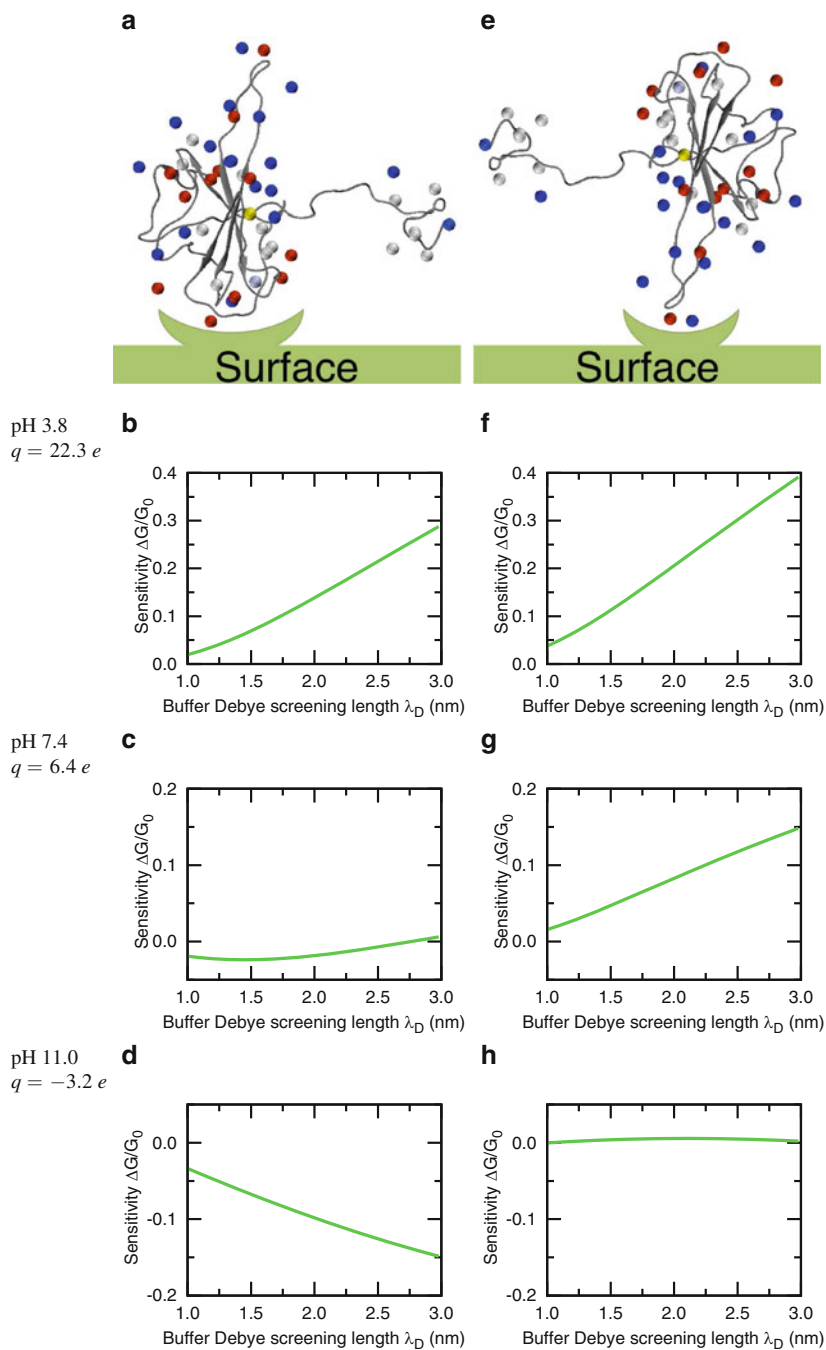


Fig. 3.11 N-protein sensing. The protein can be captured in (a) up or (e) down orientations. Different signals when varying the Debye screening length from 1 to 3 nm are expected at the different pH values 3.8, 7.4, and 11.0: (b), (c), and (d), respectively, for the up orientation and (f), (g), and (h), respectively, for the down orientation

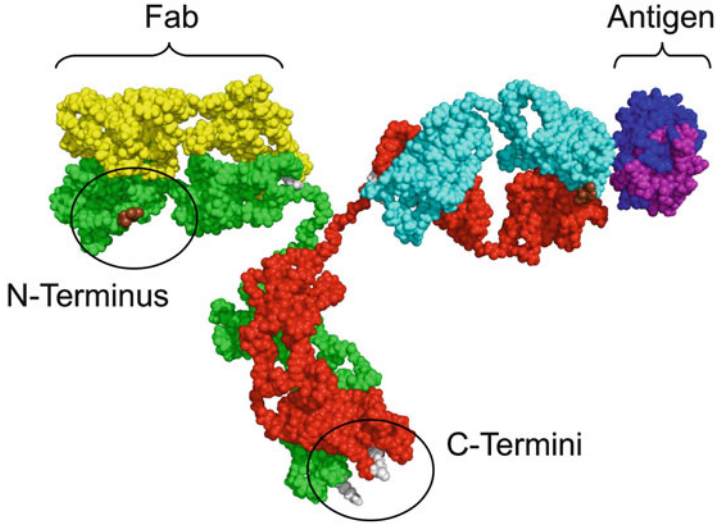


Fig. 3.12 The employed custom-prepared antibody–antigen complex. Different chains are represented with different colors. Moreover, the C-termini at the antibody base are highlighted in *gray* and the N-termini on Fab in *brown*. Figure originally from [34]: [doi:10.1371/journal.pone.0045379.g006](https://doi.org/10.1371/journal.pone.0045379.g006)

3.4.3.1 Theoretical Background

The interface was employed using the multiple charges formalism to take in consideration the different charges of the antigen and the possible effect on the simulated signal of their different orientations. However given the complexity of the studied system the following data treatment was performed through the single charge model formalism. In the following equations l stands for the average distance of the sensed charges from the nanowire surface.

As described in Sects. 3.2.1 and 3.2.3, the base conductance and conductance sensitivity can be described through (3.2) and (3.6). Since the physical and geometrical properties of the nanowire are fixed throughout all the following simulations, G_0 can be considered as constant. It is then possible to express the change in conductivity as:

$$\Delta G = K \Gamma \Gamma_l \sigma_b \quad (3.27)$$

where K collects all constant values. We define λ_D^{\max} as the value of the buffer Debye length that we consider as maximum dilution. The maximum change in conductivity at this value is:

$$\Delta G^{\max} = K \Gamma^{\max} \Gamma_l^{\max} \sigma_b \quad (3.28)$$

where we assume that changing the buffer dilution does not affect the number of adsorbed analyte molecules even at maximum dilution, hence σ_b is the same as in (3.27). Considering a highly diluted buffer, i.e. $\lambda_D^{\max} \gg l$, and substituting in (3.8) we can express Γ_l^{\max} as:

$$\Gamma_l^{\max} \simeq 2 \frac{r_{\text{nw}}}{r_{\text{nw}} + l} \left(1 + \sqrt{\frac{r_{\text{nw}}}{r_{\text{nw}} + l}} \right)^{-1} \quad (3.29)$$

The ratio between the change in conductivity at a given Debye length and the maximum possible value is:

$$\frac{\Delta G}{\Delta G^{\max}} = \frac{K \Gamma \Gamma_l \sigma_b}{K \Gamma^{\max} \Gamma_l^{\max} \sigma_b} = \frac{\Gamma \Gamma_l}{\Gamma^{\max} \Gamma_l^{\max}} \quad (3.30)$$

and after reordering it is possible to obtain:

$$\frac{\Delta G \Gamma^{\max}}{\Delta G^{\max} \Gamma} = \frac{\Gamma_l}{\Gamma_l^{\max}} \quad (3.31)$$

After inserting the explicit expressions, we obtain

$$\frac{\Gamma_l}{\Gamma_l^{\max}} = \frac{2 \frac{r_{\text{nw}}}{r_{\text{nw}} + l} \left(1 + \sqrt{\frac{r_{\text{nw}}}{r_{\text{nw}} + l}} \exp(l/\lambda_D) \right)^{-1}}{2 \frac{r_{\text{nw}}}{r_{\text{nw}} + l} \left(1 + \sqrt{\frac{r_{\text{nw}}}{r_{\text{nw}} + l}} \right)^{-1}} \quad (3.32)$$

where we define Γ_l/Γ_l^{\max} as the *relative sensitivity factor*. According to (3.32) the relative sensitivity factor depends solely on the Debye length of the simulated buffer and the average distance of the sensed charges, once chosen a value for the nanowire radius.

Using (3.5) it is possible to compute the values of Γ for different Debye lengths, including Γ^{\max} for $\lambda_D^{\max} = 1,000$ nm. In practice, the command line version of BioFET-SIM was employed to obtain these values. The BioFET-SIM parameters were set as in Table 3.1. With these parameters we obtained $G_0 = 279.0$ nS.

Using BioFET-SIM one obtains the value of ΔG (and ΔG^{\max}) simply by multiplying $\frac{\Delta G}{G_0}$ with G_0 . It is then possible to plot the l.h.s. of (3.31) for different values of λ_D . This plot is to be fitted to the r.h.s. of (3.32) where l is the fitting parameter. From a series of measures at different Debye lengths, the average distance l of the sensed charge from the nanowire surface is obtained.

3.4.3.2 Antibody and Antigen Preparation

A suitable complex structure of a generic antibody and an antigen as used by Vacic et al. [4] was prepared. Only few full antibody structures have been resolved by X-ray crystallography. We used the structure of an intact IgG2a monoclonal antibody, ascension code 11GT [65]. For the antigen we used the structure of the SEA domain of human mucin 1, with ascension code MUC1 [66].

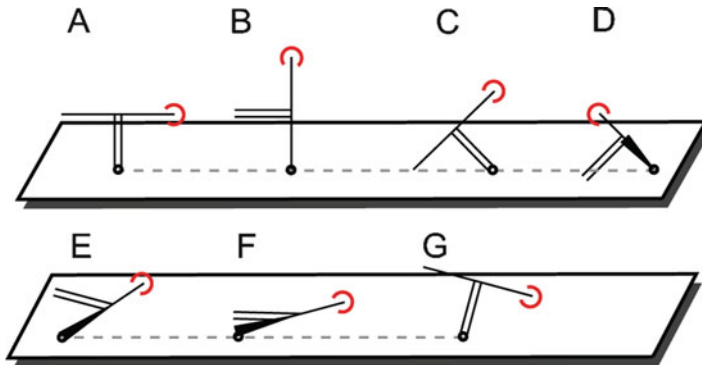


Fig. 3.13 Different orientations of the antibody with respect to the nanowire surface were considered in this study. The antigen is indicated by a *red arc*. The antibody base is indicated by a *double line*. The point of binding between the antibody and biofet surface is indicated by a *small circle*. In orientations A, C, and G the antibody is bound through the C-termini. In orientations B, D, E, and F the antibody is bound through the N-terminus. Figure originally from [34]: doi:10.1371/journal.pone.0045379.g007

The antigen structure was rigidly docked to the antigen-binding site of the antibody through the program AutoDock [67] and visually checked with the program PyMol [64] for a reasonable docking. The scope of this docking was only to obtain a feasible complex structure. The antibody–antigen complex is shown in Fig. 3.12.

Since interested in sensing only the antigen, we made the antibody structure as neutral as possible. All positions in the antibody sequence were changed to glycine using PyMol. Only the side chains were changed, while the backbone spatial disposition was maintained as in the original structure. When BioFET-SIM computes the charges of a protein it assigns a positive charge to the N termini and a negative one to the C termini, according to the PROPKA results. For this reason we changed the four chains N termini to aspartic acids and the C termini to arginines, in order to counterbalance these charges. By using a complex between the neutral antibody and the chosen antigen, we ensured that the simulated signal originated only from the antigen charges.

3.4.3.3 Antibody Orientations

Thanks to the graphical web interface, different orientations of the antibody–antigen complex were tested, simulating binding through the C- or N-termini. The seven orientations that were taken in consideration in this study are reported in Fig. 3.13. Orientations A to C correspond to those considered in [4], while orientations D to G were specifically conceived for this study. The antibody is supposedly bound to the biofet surface through the C-termini in orientations A, C, and G. Conversely, in orientations B, D, E, and F binding is through the N-terminus. C-termini binding

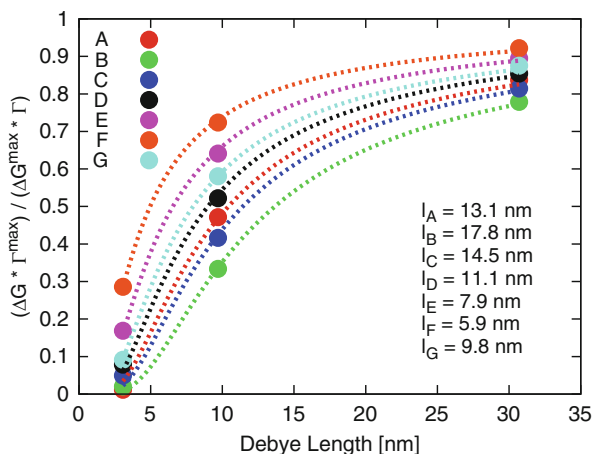


Fig. 3.14 Relative sensitivity factors for the different orientations depending on the Debye length. The computed fitting parameters l are also reported for each orientation

restricts the possible movement of the antibody with respect to the nanowire surface (the antibody remains upright), while binding through the Fab N-terminus allows more freedom of movement (the antibody can nearly lie down on the surface).

3.4.3.4 Antigen Sensing

Different orientations of the neutral antibody–antigen complex were tested, as reported in Fig. 3.13. A biofunctionalization layer of 0.5 and 1.0 nm was added for C- and N-termini binding to the nanowire surface, respectively. We considered a pH of 7.4 and kept fixed the number of proteins to 4,000. The raw data for the BioFET-SIM results for all the orientations for the values of Debye length employed by Vacic et al. (3.07, 9.7 and 30.7 nm) plus $\lambda_D^{\max} = 1,000$ nm, together with the computed data for the relative sensitivity factor are reported in the supporting material of [34] (doi:10.1371/journal.pone.0045379.s005). Here we present in Fig. 3.14 the plot of the computed relative sensitivity factor for the different orientations, together with the fitting parameters.

Among the orientations relative to C-termini binding, orientation G ($l_G = 9.8$ nm) results in an average antigen–surface distance most similar to the reported experimental value (8.4 nm). For N-terminus binding, orientations E and F ($l_E = 7.9$, $l_F = 5.9$ nm) give an average distance close to the experimental value (5.9 nm). Thus it is possible to postulate that an upright or slightly inclined orientation is preferred for C-termini binding, while when binding through one of the Fab N-termini the antibody is likely to be nearly flat on the biofet surface. Moreover, an orientation like C is quite unlikely ($l_C = 14.5$ nm), as opposed to what suggested in [4].

3.5 Conclusions

BioFET-SIM is a simple but yet powerful tool for the qualitative evaluation of nanowire-based biosensor signals. Its main characteristic is a web interface that permits any user to set up a calculation with a few mouse clicks. Most of all, the graphical interface permits to explore the effect of different orientations of the sensed analyte on the simulated signal. The graphical interface also prepares input files for the command line version of BioFET-SIM, which in turn permits to easily run batch simulations varying any given parameter.

In this chapter we showed the theoretical basis for BioFET-SIM, both in its single charge (Sect. 3.2.3) and multiple charges (Sect. 3.2.4) implementation. This was followed by an explanation of basic usage of the method (Sect. 3.3), where we showed how to study the possible effects of changing a device parameter like the oxide layer thickness on the biofet signal (Sect. 3.3.3).

Among the possible applications of BioFET-SIM we showed in Sects. 3.4.1.1 and 3.4.1.2 the effect on the sensor signal of changes of the buffer solution pH or Debye screening length. As a notable application of BioFET-SIM we mentioned the possibility of simulating a qualitative calibration curve for the signal upon sensing an analyte in different concentrations (Sect. 3.4.1.3). In Sect. 3.4.2.2 we showed the importance of using a multiple charges description of an analyte when different relative orientations of the analyte with respect to the nanowire surface are possible. We demonstrated how, through BioFET-SIM, it is possible to predict the possible signal for different orientations at different buffer pH values. Finally, in Sect. 3.4.3 we showed a complex application of BioFET-SIM aimed at interpreting and rationalizing experimental data. We demonstrated how it is possible to use the graphical web interface to prepare a series of different orientations of an antibody–antigen complex. Consequently the computed data let us postulate which of the considered orientations are those most likely to happen.

Acknowledgments This work has been partially funded by the Danish Research Council for Technology and Production Sciences (FTP), the Danish Natural Science Research Council (FNU), and by UNIK Synthetic Biology program, funded by the Danish Ministry for Science, Technology and Innovation. The authors acknowledge fruitful discussions with Lars Iversen, Noémie Loret, Rune S. Frederiksen, and Shivendra Upadhyay.

References

1. Thévenot, D.R., Toth, K., Durst, R.A., Wilson, G.S.: Electrochemical biosensors: recommended definitions and classification. *Biosens. Bioelectron.* **16**(1–2), 121 (2001). DOI 10.1016/S0956-5663(01)00115-4
2. Hermanson, G.T.: *Bioconjugate Techniques*. Academic, San Diego (1996)
3. Stern, E., Klemic, J.F., Routenberg, D.A., Wyrembak, P.N., Turner-Evans, D.B., Hamilton, A.D., LaVan, D.A., Fahmy, T.M., Reed, M.A.: Label-free immunodetection with CMOS-compatible semiconducting nanowires. *Nature* **445**, 519 (2007). DOI 10.1038/nature05498

4. Vacic, A., Criscione, J.M., Rajan, N.K., Stern, E., Fahmy, T.M., Reed, M.A.: Determination of molecular configuration by Debye length modulation. *J. Am. Chem. Soc.* **133**(35), 13886 (2011). DOI 10.1021/ja205684a
5. Chen, Y., Wang, X., Erramilli, S., Mohanty, P., Kalinowski, A.: Silicon-based nanoelectronic field-effect pH sensor with local gate control. *Appl. Phys. Lett.* **89**(22), 223512 (2006). DOI 10.1063/1.2392828
6. Cui, Y., Wei, Q., Park, H., Lieber, C.M.: Nanowire nanosensors for highly sensitive and selective detection of biological and chemical species. *Science* **293**, 1289 (2001). DOI 10.1126/science.1062711
7. Gao, X.P., Zheng, G., Lieber, C.M.: Subthreshold regime has the optimal sensitivity for nanowire FET biosensors. *Nano Lett.* **10**(2), 547 (2009). DOI 10.1021/nl9034219
8. Tian, R., Regonda, S., Gao, J., Liu, Y., Hu, W.: Ultrasensitive protein detection using lithographically defined Si multi-nanowire field effect transistors. *Lab Chip* **11**, 1952 (2011). DOI 10.1039/C0LC00605J
9. Wong, I.Y., Melosh, N.A.: Directed hybridization and melting of DNA linkers using counterion-screened electric fields. *Nano Lett.* **9**(10), 3521 (2009). DOI 10.1021/nl901710n
10. Dorvel, B.R., Reddy, B., Go, J., Duarte Guevara, C., Salm, E., Alam, M.A., Bashir, R.: Silicon nanowires with high-k Hafnium oxide dielectrics for sensitive detection of small nucleic acid oligomers. *ACS Nano* **6**(7), 6150 (2012). DOI 10.1021/nn301495k
11. Chang, H.K., Ishikawa, F.N., Zhang, R., Datar, R., Cote, R.J., Thompson, M.E., Zhou, C.: Rapid, label-free, electrical whole blood bioassay based on nanobiosensor systems. *ACS Nano* **5**(12), 9883 (2011). DOI 10.1021/nn2035796
12. Berthing, T., Sørensen, C.B., Nygård, J., Martinez, K.L.: Applications of nanowire arrays in nanomedicine. *J. Nanoneurosci.* **1**(1), 3 (2009). DOI 10.1166/jns.2009.001
13. Patolsky, F., Zheng, G., Lieber, C.M.: Nanowire-based biosensors. *Anal. Chem.* **78**(13), 4260 (2006). DOI 10.1021/ac069419j
14. Shinwari, M.W., Deen, M.J., Landheer, D.: Study of the electrolyte-insulator-semiconductor field-effect transistor (EISFET) with applications in biosensor design. *Microelectron. Reliab.* **47**(12), 2025 (2007). DOI 10.1016/j.microrel.2006.10.003
15. Curreli, M., Zhang, R., Ishikawa, F.N., Chang, H.K., Cote, R.J., Zhou, C., Thompson, M.E.: Real-time, label-free detection of biological entities using nanowire-based FETs. *IEEE Trans. Nanotechnol.* **7**(6), 651 (2008). DOI 10.1109/TNANO.2006.880908
16. Neizvestny, I.G.: Semiconductor nanowire sensors. *Russ. Microelectron.* **38**(4), 223 (2009). DOI 10.1134/S1063739709040015
17. Roy, S., Gao, Z.: Nanostructure-based electrical biosensors. *Nano Today* **4**(4), 318 (2009). DOI 10.1016/j.nantod.2009.06.003
18. Nair, P.R., Alam, M.A.: Performance limits of nanobiosensors. *Appl. Phys. Lett.* **88**(23), 233120 (2006). DOI 10.1063/1.2211310
19. Nair, P.R., Alam, M.A.: Screening-limited response of nanoBiosensors. *Nano Lett.* **8**(5), 1281 (2008). DOI 10.1021/nl072593i
20. Nair, P.R., Alam, M.A.: Theory of “Selectivity” of label-free nanobiosensors: A geometro-physical perspective. *J. Appl. Phys.* **107**(6), 064701 (2010). DOI 10.1063/1.3310531
21. Heitzinger, C., Klimeck, G.: Computational aspects of the three-dimensional feature-scale simulation of silicon-nanowire field-effect sensors for DNA detection. *J. Comput. Electron.* **6**, 387 (2007). DOI 10.1007/s10825-006-0139-x
22. Ringhofer, C., Heitzinger, C.: Multi - scale modeling and simulation of field-effect biosensors. *ECS Trans.* **14**(1), 11 (2008). DOI 10.1149/1.2956012
23. Heitzinger, C., Kennell, R., Klimeck, G., Mauser, N., McLennan, M., Ringhofer, C.: Modeling and simulation of field-effect biosensors (BioFETs) and their deployment on the nanoHUB. *J. Phys. Conf. Ser.* **107**, 012004 (2008). DOI 10.1088/1742-6596/107/1/012004
24. Chen, H., Mukherjee, S., Aluru, N.: Charge distribution on thin semiconducting silicon nanowires. *Comput. Methods Appl. Mech. Eng.* **197**(41–42), 3366 (2008). DOI 10.1016/j.cma.2008.02.007
25. Heitzinger, C., Mauser, N.J., Ringhofer, C., Liu, Y., Dutton, R.W.: Proceedings of the Simulation of Semiconductor Processes and Devices (SISPAD 2009) (San Diego, CA, USA, 2009), pp. 86–90 (2009). DOI 10.1109/SISPAD.2009.5290244

26. Heitzinger, C., Mauser, N.J., Ringhofer, C.: Multiscale modeling of planar and nanowire field-effect biosensors. *SIAM J. Appl. Math.* **70**(5), 1634 (2010). DOI 10.1137/080725027
27. Windbacher, T., Sverdlov, V., Selberherr, S.: Biomedical engineering systems and technologies. In: Fred, A., Filipe, J., Gamboa, H. (eds.) *Communications in Computer and Information Science*, vol. 52, pp. 85–95. Springer, Berlin (2010). DOI 10.1007/978-3-642-11721-3{_}6
28. Park, H.H., Zeng, L., Buresh, M., Wang, S., Klimeck, G., Mehrotra, S.R., Heitzinger, C., Haley, B.P.: Nanowire. NanoHUB website (2006). DOI 10254/nanohub-r1307.8. URL <http://nanohub.org/resources/1307>. Accessed Mar 2013
29. Nair, P.R., Go, J., Landells, G.J., Pandit, T.R., Alam, M.A.: BioSensorLab, NanoHUB website (2008). DOI 10254/nanohub-r2929.5. URL <http://nanohub.org/resources/2929>. Accessed Mar 2013
30. Medici: Two Dimensional Device Simulation Program (2003). Synopsis
31. Sørensen, M.H., Mortensen, N.A., Brandbyge, M.: Screening model for nanowire surface-charge sensors in liquid. *Appl. Phys. Lett.* **91**(10), 102105 (2007). DOI 10.1063/1.2779930
32. De Vico, L., Sørensen, M.H., Iversen, L., Rogers, D.M., Sørensen, B.S., Brandbyge, M., Nygård, J., Martinez, K.L., Jensen, J.H.: Quantifying signal changes in nano-wire based biosensors. *Nanoscale* **3**, 706 (2011). DOI 10.1039/C0NR00442A
33. De Vico, L., Iversen, L., Sørensen, M.H., Brandbyge, M., Nygård, J., Martinez, K.L., Jensen, J.H.: Predicting and rationalizing the effect of surface charge distribution and orientation on nano-wire based FET bio-sensors. *Nanoscale* **3**, 3635 (2011). DOI 10.1039/C1NR10316D
34. Hediger, M.R., Jensen, J.H., De Vico, L.: BioFET-SIM Web Interface: Implementation and Two Applications. *PLoS One* **7**(10), e45379 (2012). DOI 10.1371/journal.pone.0045379
35. Punzet, M., Baurecht, D., Varga, F., Karlic, H., Heitzinger, C.: Determination of surface concentrations of individual molecule-layers used in nanoscale biosensors by in situ ATR-FTIR spectroscopy. *Nanoscale* **4**, 2431 (2012). DOI 10.1039/C2NR12038K
36. Hakim, M.M.A., Lombardini, M., Sun, K., Giustiniano, F., Roach, P.L., Davies, D.E., Howarth, P.H., de Planque, M.R.R., Morgan, H., Ashburn, P.: Thin film polycrystalline silicon nanowire biosensors. *Nano Lett.* **12**(4), 1868 (2012). DOI 10.1021/nl2042276
37. Duan, X., Li, Y., Rajan, N., Routenberg, D., Modis, Y., Reed, M.: Quantification of the affinities and kinetics of protein interactions using silicon nanowire biosensors. *Nat. Nanotechnol.* **7**(6), 401 (2012). DOI 10.1038/nnano.2012.82
38. Elnathan, R., Kwiat, M., Pevzner, A., Engel, Y., Burstein, L., Khatchourints, A., Lichtenstein, A., Kantaev, R., Patolsky, F.: Biorecognition layer engineering: Overcoming screening limitations of nanowire-based FET devices. *Nano Lett.* **12**(10), 5245 (2012). DOI 10.1021/nl302434w
39. Lloret, N., Frederiksen, R.S., Møller, T.C., Rieben, N.I., Upadhyay, S., De Vico, L., Jensen, J.H., Nygård, J., Martinez, K.L.: Effects of buffer composition and dilution on nanowire field-effect biosensors. *Nanotechnology* **24**(3), 035501 (2013). DOI 10.1088/0957-4484/24/3/035501
40. Magliulo, M., Mallardi, A., Mulla, M.Y., Cotrone, S., Pistillo, B.R., Favia, P., Vikholm-Lundin, I., Palazzo, G., Torsi, L.: Electrolyte-gated organic field-effect transistor sensors based on supported biotinylated phospholipid bilayer. *Adv. Mater.* **25**(14), 2090 (2013). DOI 10.1002/adma.201203587
41. Hammock, M.L., Knopfmacher, O., Naab, B.D., Tok, J.B.H., Bao, Z.: Investigation of protein detection parameters using nanofunctionalized organic field-effect transistors. *ACS Nano* **7**(5), 3970 (2013). DOI 10.1021/nm305903q
42. Baumgartnerth, S., Heitzinger, C., Vacic, A., Reed, M.A.: Predictive simulations and optimization of nanowire field-effect PSA sensors including screening. *Nanotechnology* **24**(22), 225503 (2013). DOI 10.1088/0957-4484/24/22/225503
43. Nitzan, A., Galperin, M., Ingold, G.L., Grabert, H.: On the electrostatic potential profile in biased molecular wires. *J. Chem. Phys.* **117**(23), 10837 (2002). DOI 10.1063/1.1522406
44. Liang, G.C., Ghosh, A.W., Paulsson, M., Datta, S.: Electrostatic potential profiles of molecular conductors. *Phys. Rev. B* **69**, 115302 (2004). DOI 10.1103/PhysRevB.69.115302

45. Zhang, X.G., Pantelides, S.T.: Screening in nanowires and nanocontacts: Field emission, adhesion force, and contact resistance. *Nano Lett.* **9**(12), 4306 (2009). DOI 10.1021/nl902533n, PMID: 19845331
46. Sørensen, M.H.: Nanowires for chemical sensing in a liquid environment. Bachelor Thesis (2007)
47. Olver, F.W.J.: In: Abramowitz, M., Stegun, I.A. (eds.) *Handbook of Mathematical Functions with Formulas, Graphs, and Mathematical Tables*, pp. 355–436. Dover, New York (1973)
48. Ishikawa, F.N., Chang, H.K., Curreli, M., Liao, H.L., Olson, C.A., Chen, P.C., Zhang, R., Roberts, R.W., Sun, R., Cote, R.J., Thompson, M.E., Zhou, C.: Label-free, electrical detection of the SARS virus N-protein with nanowire biosensors utilizing antibody mimics as capture probes. *ACS Nano* **3**(5), 1219 (2009). DOI 10.1021/nn900086c
49. Björk, M.T., Schmid, H., Knoch, J., Riel, H., Riess, W.: Donor deactivation in silicon nanostructures. *Nat. Nanotechnol.* **4**(2), 103 (2009). DOI 10.1038/nnano.2008.400
50. Garnett, E.C., Tseng, Y.C., Khanal, D.R., Wu, J., Bokor, J., Yang, P.: Dopant profiling and surface analysis of silicon nanowires using capacitance–voltage measurements. *Nat. Nanotechnol.* **4**(5), 311 (2009). DOI 10.1038/nnano.2009.43
51. Stern, E., Wagner, R., Sigworth, F.J., Breaker, R., Fahmy, T.M., Reed, M.A.: Importance of the Debye screening length on nanowire field effect transistor sensors. *Nano Lett.* **7**(11), 3405 (2007). DOI 10.1021/nl071792z
52. Nair, P.R., Alam, M.A.: Design considerations of silicon nanowire biosensors. *IEEE Trans. Electron Devices* **54**(12), 3400 (2007). DOI 10.1109/TED.2007.909059
53. Yates, D.E., Levine, S., Healy, T.W.: Site-binding model of the electrical double layer at the oxide/water interface. *J. Chem. Soc. Faraday Trans. 1* **70**, 1807 (1974). DOI 10.1039/F19747001807
54. Li, H., Robertson, A.D., Jensen, J.H.: Very fast empirical prediction and rationalization of protein pK_a values. *Proteins Struct. Funct. Bioinforma.* **61**(4), 704 (2005). DOI 110.1002/prot.20660
55. Bas, D.C., Rogers, D.M., Jensen, J.H.: Very fast prediction and rationalization of pK_a values for protein-ligand complexes. *Proteins Struct. Funct. Bioinforma.* **73**(3), 765 (2008). DOI 10.1002/prot.22102
56. Olsson, M.H.M., Søndergaard, C.R., Rostkowski, M., Jensen, J.H.: PROPKA3: Consistent treatment of internal and surface residues in empirical pK_a predictions. *J. Chem. Theory Comput.* **7**(2), 525 (2011). DOI 10.1021/ct100578z
57. Ullmann, G.M., Knapp, E.W.: Electrostatic models for computing protonation and redox equilibria in proteins. *Eur. Biophys. J.* **28**, 533 (1999). DOI 10.1007/s002490050236
58. Berman, H.M., Westbrook, J., Feng, Z., Gilliland, G., Bhat, T.N., Weissig, H., Shindyalov, I.N., Bourne, P.E.: The protein data bank. *Nucleic Acids Res.* **28**(1), 235 (2000). DOI 10.1093/nar/28.1.235
59. Liu, Y., Rieben, N., Iversen, L., Sørensen, B., Park, J., Nygård, J., Martinez, K.: Specific and reversible immobilization of histidine-tagged proteins on functionalized silicon nanowires. *Nanotechnology* **21**, 245105 (2010). DOI 10.1088/0957-4484/21/24/245105
60. Pugliese, L., Coda, A., Malcovati, M., Bolognesi, M.: Three-dimensional structure of the tetragonal crystal form of egg-white avidin in its functional complex with biotin at 2.7 Å resolution. *J. Mol. Biol.* **231**(3), 698 (1993). DOI 10.1006/jmbi.1993.1321
61. Weber, P., Ohlendorf, D., Wendoloski, J., Salemme, F.: Structural origins of high-affinity biotin binding to streptavidin. *Science* **243**(4887), 85 (1989). DOI 10.1126/science.2911722
62. Green, N.M.: Avidin-biotin technology. In: Wilchek, M., Bayer, E.A. (eds.) *Methods in Enzymology*, vol. 184, pp. 51–67. Academic, London (1990). DOI 10.1016/0076-6879(90)84259-J
63. Hediger, M.R.: A perspective on bionanosensor simulation & computational enzyme engineering. Ph.D. Thesis, Department of Chemistry, University of Copenhagen (2013)
64. The PyMOL Molecular Graphics System: Version 1.3.0 Schrödinger, LLC
65. Harris, L.J., Larson, S.B., Hasel, K.W., McPherson, A.: Refined structure of an intact IgG2a monoclonal antibody. *Biochemistry* **36**(7), 1581 (1997). DOI 10.1021/bi962514+

66. Macao, B., Johansson, D., Hansson, G., Härd, T.: Autoproteolysis coupled to protein folding in the SEA domain of the membrane-bound MUC1 mucin. *Nat. Struct. Mol. Biol.* **13**(1), 71 (2005). DOI 10.1038/nsmb1035
67. Goodsell, D.S., Morris, G.M., Olson, A.J.: Automated docking of flexible ligands: Applications of autodock. *J. Mol. Recognit.* **9**(1), 1 (1996). DOI 10.1002/(SICI)1099-1352(199601)9:1<1::AID-JMR241>3.0.CO;2-6